An Experimental Study of Massive MIMO Properties in 5G Scenarios

Martinez, Alex Oliveras; Nielsen, Jesper Ødum; Carvalho, Elisabeth De; Popovski, Petar

Published in:
I E E E Transactions on Antennas and Propagation

DOI (link to publication from Publisher):
10.1109/TAP.2018.2871881

Publication date:
2018

Document Version
Accepted author manuscript, peer reviewed version

This article has been accepted for publication in a future issue of this journal, but has not been fully edited. Content may change prior to final publication. Citation information: DOI 10.1109/TAP.2018.2871881, IEEE Transactions on Antennas and Propagation

An Experimental Study of Massive MIMO Properties in 5G Scenarios

Àlex Oliveras Martínez, Jesper Ødum Nielsen, Elisabeth De Carvalho, and Petar Popovski

***Abstract*—Three main characteristics of massive multiple-input-multiple-output (MIMO) are studied. The wide-spread use of these characteristics and their lack of validation motivates this study based in measurements. First we study the channel hardening when the number of antennas in the base station (BS) increases. Second we focus on the channel vector orthogonality between two users. Third we investigate the rank of the spatial covariance matrix. The data used for this research has been obtained in two measurement campaigns with all real antennas (i.e. neither virtual arrays nor virtual users). The first one has 64 BS elements arranged in 3 configurations, and it serves 8 users with 2 antennas each. The second campaign has 128 BS elements, serving 2 users with 2 antennas each. Both campaigns include line-of-sight (LoS) and non-line-of-sight (NLoS) scenarios, designed according to the future 5G deployment scenarios. We show the rate of channel hardening when the number of BS elements increases. We evaluate the sum-rate of two users at specific distances between them. We observe the large angular spread occupied by the user.**

***Index Terms*—massive MIMO, multi-user MIMO, channel measurements, linear antenna arrays.**

I. Introduction

THE current growth in the number of mobile phones and other connected devices demands high data throughputs. The existing cellular systems fall behind the needed performance. Next generation wireless solutions will need to meet the increasing demand of capacity, reliability and energy efficiency. Massive MIMO tackles these requirements, thus, in the recent years, has attracted a lot of attention as an enabling technology for the next generations of communications systems (e.g. 5G [1]). The seminal work of Marzetta [2] describes it as a BS comprising a very large number of elements serving a much smaller number of single antenna terminals in the same time-frequency resource.

The benefits of massive MIMO have been extensively studied in theoretical channels but also in measurements. However, due to the difficulties to measure such a large number of antennas simultaneously, most of the measurements utilize virtual antennas to create the BS array [3]–[9]. However, some papers study measurements with real arrays [10]–[12] and some studies compare virtual and real arrays [13], [14]. Simulatenous user measurements are reported in [12]. Some papers describe outdoor scenarios [3]–[7], [11]–[14], some indoor scenarios [8], [9], [11]and some outdoor-indoor [10]. Most of the measurements have 64 antenna ports [6], [8], [11] or 128 [3], [5], [10], [12]–[14], with the exception of [4] that has 112, [7] that has 256 and [9] that has 400.

There are three determining topics for massive MIMO performance that have only been derived from simplified theoretical models. Here we would like to verify them experimentally:

1) Channel hardening: The superior number of BS elements with respect to users leaves degrees of freedom unused. The excess of degrees of freedom can be used to reduce fast fading and average out noise due to the law of large numbers. This effect is called channel hardening because the channel becomes more stable. This may not happen (or happen to less degree) in measured channels because the channels are not independent as needed for the law of large numbers to be effective.

2) Users' channel vector orthogonality: When the number of BS elements grows large the channel vector of two users becomes asymptotically orthogonal. This result allows to eliminate the inter-user (or intra-cell) interference. But the orthogonality between users' channel vectors strongly depends on their relative position. Two users close to each other, are inside the same radiation pattern beam (in LoS) or they see the same scatterers (in NLoS). As a result their channel vectors can be similar, and the orthogonality is affected.

3) Rank of the spatial covariance matrix: Some methods for multicell pilot contamination avoidance, channel estimation [15] and FDD transmission [16] assume low rank of the covariance matrix because the large aperture of the array in massive MIMO achieves very narrow beams and in absence of scatterers these narrow beams render a sparse covariance channel matrix. This is different from the rank of the instantaneous multi-user channel matrix that has been studied in other measurements [17]. However, studies on direction of arrivals can be found which are related to rank of the spatial covariance matrix [3], [6].

These three properties are studied from a channel characterisation perspective instead of a massive MIMO performance perspective. These allows us to abstract from specific transmission techniques and we can present general properties of the channel useful in a broader range of applications.

The following study uses the data of two measurement campaigns to analyze the three previously mentioned topics. Both measurements are conducted at $5.8\,\mathrm{GHz}$. The first one has 64 BS real elements reconfigurable into three array shapes: A very long aperture ($6\,\mathrm{m}$) array, a long aperture ($2\,\mathrm{m}$) array, and a rectangular ($25\,\mathrm{cm}$ by $28\,\mathrm{cm}$) array. This array serves 8 users with 2 antennas each. Line-of-Sight (LoS) and Non-Line-of-Sight (NLoS) scenarios are measured. We focus on

Faculty of Engineering and Science, Dept. of Electronic Systems, APNet section, Aalborg University, Aalborg, Denmark, E-mail: {aom,jni,edc,petarp}@es.aau.dk

This article has been accepted for publication in a future issue of this journal, but has not been fully edited. Content may change prior to final publication. Citation information: DOI 10.1109/TAP.2018.2871881, IEEE Transactions on Antennas and Propagation

indoor scenarios where moving users hold a handset mockup. The second campaign has 128 real BS elements serving 2 users with 2 antennas each. The scenario is outdoors and includes both LoS and NLoS. The data of the measurements was first analyzed in [17]–[19]. The location of the measurements is carefully chosen, envisioning new scenarios for the 5G wireless systems (i.e. large indoor spaces such as shopping malls, large venues, sport stadiums, etc. See [1] Chapter 2). Such scenarios can integrate very large BS arrays into their structures. We focus on such scenarios because their high user density represents a challenge for the next generation of wireless systems.

The previously published results revealed the orthogonality of arbitrarily located users, the degrees of freedom in the form of normalized sum of eigenvalues, the condition number of the channel matrix and power non-stationarities across the array [17], [18].

In this publication the analysis of the data from these campaigns shows us the hardening of the channel when the number of BS antennas increases. We see that larger apertures induce more hardening. However, the hardening is less than in the Gaussian channels. The Gaussian channel is defined for the rest of the paper as a channel with independent identically distributed complex Gaussian entries with zero mean and unit variance. We also observe that the correlation between users is tightly related to their relative position in NLoS and strongly depends on the radiation pattern in LoS. Finally we show the rank of the spatial covariance matrix and its impact on the channel hardening. In [19] these metrics were presented only in specific scenarios and users, while in this publication these results are presented with the statistics over all the scenarios and arrays used in the measurements[1]. In addition we present the impact of the users' distance-specific correlation to the matched filter sum rate and we compare it with a simulated channel. We also show the beamforming angle of arrival averaged over channel realizations for several scenarios and users.

II. Measurement campaigns

A. 5G scenarios

The first measurement campaign uses 64 BS elements and we call it 64-mMIMO. The measurement campaign was carried out at Aalborg University in a large indoor environment similar to a shopping mall with a staircase in the middle of the room. This location was chosen to study a 5G scenario called *shopping mall* in [1] Chapter 2.

The second measurement campaign uses 128 BS elements and we call it 128-mMIMO. The measurement campaign was carried out in an outdoor scenario at Aalborg University, Denmark. The environment has a large grass field in the center surrounded by buildings three floors high. In one side there is a road and a parking lot between the field and the building. LoS measurements are conducted in the middle of the field (at $30\,\mathrm{m}$ from the BS) and NLoS measurements are conducted outside the field, behind a group of trees (at $60\,\mathrm{m}$ from the BS). This location was chosen to study a 5G scenario called *large outdoor event* in [1] Chapter 2.

[1]Unfortunately, an erroneous scaling was applied in the channel hardening study of [19]. In [19] a varying transmit power is considered using a scaling (i.e. $\frac{M}{M'}$ where M is the total number of antennas and M' is the selected number of antennas) in order to compensate for the array gain (i.e. the array gain is proportional to M'). Note that the scaling with $\frac{M}{M'}$ was not mentioned in [19]. However, this scaling is wrong since the array gain is already compensated by normalizing to the average power across the BS antennas. The average power per antenna is $\frac{P_T}{M'}$, where P_T is the sum power, and hence the array gain M' is effectively compensated twice, making the overall scaling wrong.

	LoS	NLoS
Spread Users	**(S-LoS ‖) (S-LoS ⊥)**	**(S-NLoS)**
Grouped Users	**(G-LoS)**	**(G-NLoS)**
Without Users	**(F-InFront) (F-Behind)**	

TABLE I
Scenario reference table.

B. 64-*mMIMO*

This section outlines the main characteristics of 64-mMIMO. For more details refer to [17].

1) Three massive array shapes: Three BS arrays are tested, all consisting of 64 monopole elements. The monopoles are arranged in eight linear arrays, named sets in the following.

The array sets are grouped in three dispositions, shown in Fig. 1:

VLA: The very large aperture array is $6\,\mathrm{m}$ long where the antenna sets are placed longitudinally separated $50\,\mathrm{cm}$.

LA: The large aperture array is $2\,\mathrm{m}$ long where the antenna sets are placed longitudinally without separation.

C2D: The compact 2D array is a rectangular array of $25\,\mathrm{cm}$ by $28\,\mathrm{cm}$ where the antenna sets are placed next to each other, along the long edges.

2) Eight handsets with two antennas: The measurements involve eight mock-up handsets with four antennas (one at each corner), but only the two antennas in the top are active. The antennas are monopole-like with polarization in the plane of the handset along the larger dimension of the handset. Fig. 2 shows the handset.

Eight users hold the handsets in front of them as if using a smartphone for browsing. The handsets are tilted about forty-five degrees with respect to the ground, with random variations due to the users. During the measurements the users move the handset randomly in a $1\,\mathrm{m}^2$ area to generate small-scale changes in the channel.

3) Seven scenarios: In the following, *scenarios* denote the dispositions of the users or handsets. Seven scenarios are tested, each one with specific propagation properties, with LoS and NLoS and with a specific distribution of the devices. Table I summarizes the scenarios. Some scenarios are depicted in Fig. 3. Fig. 4 shows a floor map of some scenarios. Notice that $\|$ refers to scenarios where the two antennas in the handset form an array parallel to the BS. On the other hand $\perp$ means that the two antennas of the handset form an array perpendicular to the BS. F-InFront means that the handsets are deployed in front of the stairs, while F-Behind means the handsets are behind the stairs. A more detailed description of the scenarios can be found in [17].

This article has been accepted for publication in a future issue of this journal, but has not been fully edited. Content may change prior to final publication. Citation information: DOI 10.1109/TAP.2018.2871881, IEEE Transactions on Antennas and Propagation

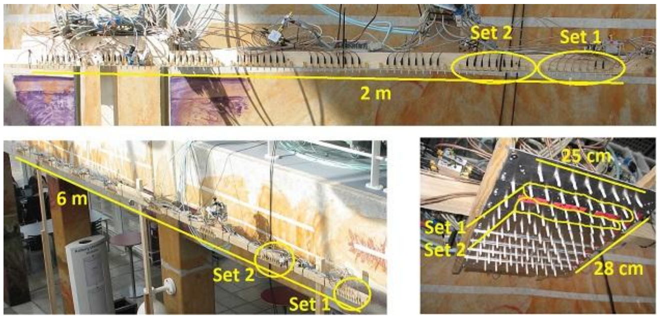

Fig. 1. Antenna configurations. Bottom-left: VLA, Top: LA and Bottom-right: C2D

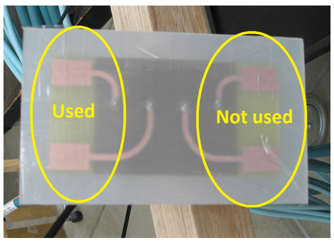

Fig. 2. Handset with four antennas. Only two are used

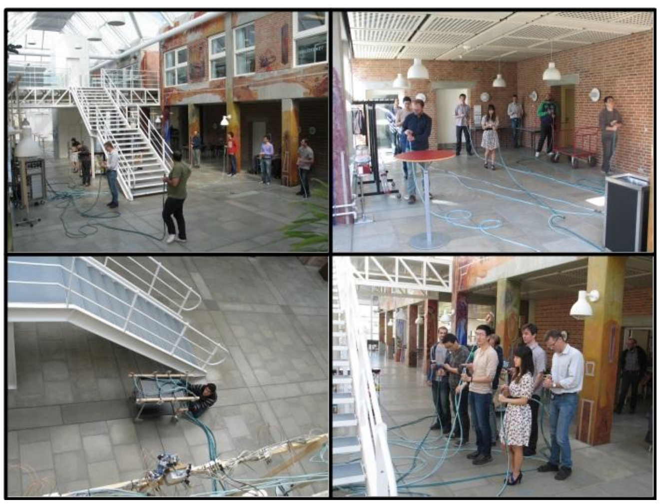

Fig. 3. Top-left, S-LoS ||. Top-right, S-NLoS. Bottom-left, F-InFront. Bottom-right, G-LoS

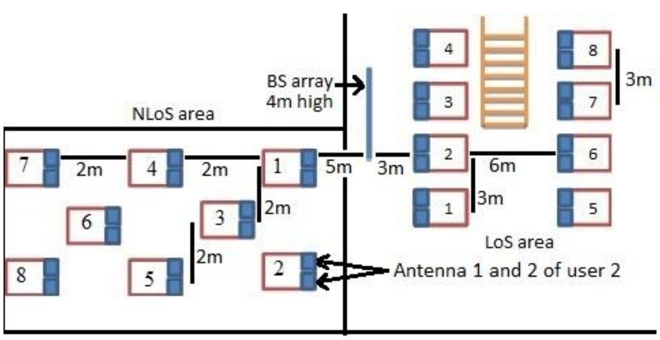

Fig. 4. Floor map with location of BS array, LoS area, NLoS area and user numbering.

C. 128-*mMIMO*

This section outlines the main characteristics of 128-mMIMO.

1) Base station array: The BS array consists of 128 monopole elements. The monopoles are arranged in eight linear arrays, named sets in the following, each with sixteen elements separated by $\lambda/2$. Two dummy monopoles are added at the ends of each set so that all the active elements have similar properties. The sets are separated $0.34\,\mathrm{m}$. The total length of the BS is $5.78\,\mathrm{m}$ and it is placed on the wall at approx. $4.1\,\mathrm{m}$ from the ground. Fig. 5 shows the BS array.

2) Two scenarios: In the following *scenarios* denote the dispositions of the users. Two scenarios are tested, LoS and NLoS. Fig. 6 show the two scenarios and their relative position to the BS.

3) Two handsets with two antennas: The measurements involve two mock-up handsets (the same as in the first campaign, showed in Fig. 2). Two users hold the handsets in front of them as if using a smartphone for browsing. They are allowed to have their own hand-grip to make the measurements more realistic. The users move the mock-up randomly in a $1\,\mathrm{m}^2$ area (i.e. approx. 20×20 wavelengths) to generate small-scale changes in the channel. In order to control the mean distance between users a $1.1\,\mathrm{m}$ stick is used. One end of the stick is placed in fixed positions marked on the ground, and the other end is held and moved by the users together with the mock-up. The stick can be seen in the hands of user 1 in Fig. 7. The mean distance between users is modified by changing the position of the lower end of the stick. The positions marked on the ground are represented with blue dots in Fig. 6.

1) LoS scenario: The users increase their separation in the parallel dimension of the array. The users are measured in 10 positions separated by: $0.2\,\mathrm{m}$, $0.3\,\mathrm{m}$, $0.4\,\mathrm{m}$, $0.5\,\mathrm{m}$, $0.6\,\mathrm{m}$, $0.8\,\mathrm{m}$, $1\,\mathrm{m}$, $1.5\,\mathrm{m}$, $2\,\mathrm{m}$, and $4\,\mathrm{m}$.
2) NLoS scenario: Each user is located on one of two orthogonal lines. The users are measured in 21 positions separated from the crossing point by: $4\,\mathrm{m}$, $2\,\mathrm{m}$, $1.5\,\mathrm{m}$, $1\,\mathrm{m}$, $0.8\,\mathrm{m}$, $0.6\,\mathrm{m}$, $0.5\,\mathrm{m}$, $0.4\,\mathrm{m}$, $0.3\,\mathrm{m}$, $0.2\,\mathrm{m}$, $0\,\mathrm{m}$, $0.2\,\mathrm{m}$, $0.3\,\mathrm{m}$, $0.4\,\mathrm{m}$, $0.5\,\mathrm{m}$, $0.6\,\mathrm{m}$, $0.8\,\mathrm{m}$, $1\,\mathrm{m}$, $1.5\,\mathrm{m}$, $2\,\mathrm{m}$, and $4\,\mathrm{m}$.

Fig. 7 shows the two users during a measurement.

III. Channel sounder and Normalization

A. *Channel sounder: quasi-simultaneous measurements*

The measurements were made with a correlation based channel sounder operating at $5.8\,\mathrm{GHz}$ and with a bandwidth of about $100\,\mathrm{MHz}$. The sounder has 8 parallel receive channels and 16 parallel transmit channels. In the 64-mMIMO campaign the sounder measures the 8×16 MIMO channel fully in parallel, which is further extended by connecting the elements of each antenna set (defined in subsection II-B1) via a fast switch. The sounder measures the full system channel (64×16) semi-simultaneously (i.e. within $655\,\mu\mathrm{s}$), so we can consider the channel to be static during the measurement interval. This remarkable characteristic of the sounder allows the measurement of dynamic channels. In the 128-mMIMO campaign the sounder uses only a subset of the transmit ports

This article has been accepted for publication in a future issue of this journal, but has not been fully edited. Content may change prior to final publication. Citation information: DOI 10.1109/TAP.2018.2871881, IEEE Transactions on Antennas and Propagation

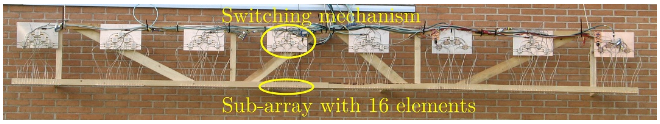

Fig. 5. BS array with 8 sets of 16 elements

(i.e. 4) so it measures a 8×4 MIMO channel fully in parallel, which is further extended by connecting the elements of each antenna set (defined in subsection II-C1) via a fast switch. The sounder measures the full system channel (128×4) semi-simultaneously (i.e. within $1.31\,\mathrm{ms}$). The massive MIMO channel is sampled at a rate of $60\,\mathrm{Hz}$ during $20\,\mathrm{s}$, for a total of 1200 channel realizations in each measurement run. The measurement SNR averaged over scenarios, arrays, users positions, and all the antenna links is estimated to be $27\,\mathrm{dB}$ and $20\,\mathrm{dB}$ for the 64-mMIMO and 128-mMIMO respectively with a 5 percentile of $13\,\mathrm{dB}$ and $6\,\mathrm{dB}$ respectively.

B. Narrowband channel and Normalization

We focus on the analysis of a narrow band channel obtained via Fourier transform of the measured impulse responses. We disregard all the frequencies except the central one with a bandwidth of $2\,\mathrm{MHz}$. We denote $\mathbf{h}_k^{(n)}(r)\in\mathbb{C}^{M\times 1}$ as the channel vector from antenna $n\in\{a,b\}$ in the handset of user $k\in\{1,...,8\}$ in 64-mMIMO and $k\in\{1,2\}$ in 128-mMIMO to the BS array at channel realization $r\in\{1,...,R\}$, where $R=1200$. $M=64$ in 64-mMIMO and $M=128$ in 128-mMIMO is the number of BS elements. $h_{mk}^{(n)}(r)$ is the mth entry of the vector, corresponding to the mth element of the BS array. We call $\mathbf{H}(r)\in\mathbb{C}^{M\times KN}$ the full 64×16 channel matrix in 64-mMIMO and 128×4 in 128-mMIMO. $K=8$ is the number of users in 64-mMIMO and $K=2$ in 128-mMIMO, $N=2$ is the number of antennas per user. The two channel vectors of user k at realization r are placed in two consecutive columns of $\mathbf{H}(r)$.

Normalizing the channel we create a virtual power gain control, where the received energy from each user antenna is normalized as:

$$\overline{\mathbf{h}}_k^{(n)}(r)=\frac{\mathbf{h}_k^{(n)}(r)}{\sqrt{\sum\limits_{r=1}^{R}\left\|\mathbf{h}_k^{(n)}(r)\right\|^2}}\sqrt{MR} \tag{1}$$

where $\|\cdot\|$ is the Euclidean norm.

With this normalization, we remove the user impact and handset antenna power imbalance but we keep the differences among BS elements. We denote $\overline{\mathbf{H}}(r)\in\mathbb{C}^{M\times KN}$ as the channel matrix made out of the normalized vectors in (1).

IV. Channel hardening

One of the most promising features of massive MIMO is its capability to harden the channel. In other words, the fast fading is reduced and the noise is averaged out as a result of the law of large numbers [20]. Channel hardening allows to allocate resources in a longer time period, since the fast variations of the channel vanishes. In addition, the signal power of each user is more stable, so the outage probability is reduced.

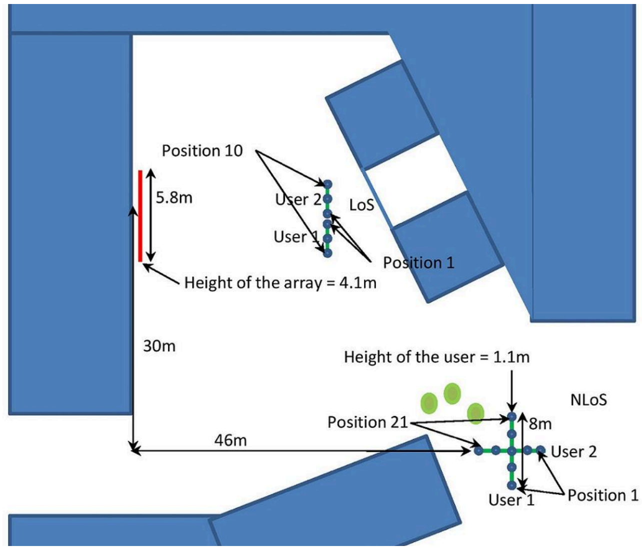

Fig. 6. Scenario in LoS and scenario in NLoS

Fig. 7. 2 users holding the sticks to keep the separation constant

A. Standard deviation of the mean power

To study the channel hardening effect, we compute the standard deviation of the mean power across the antennas of the BS array. The mean power is

$$\overline{P}_k^{(n)}(r)=\frac{1}{M'}\sum_{m=1}^{M'}\left|\overline{h}_{mk}^{(n)}(r)\right|^2 \tag{2}$$

where M' is the selected number of BS elements. The standard deviation is computed over the R realizations of the channel as

$$Std_k^{(n)}=\sqrt{\frac{\sum_{r=1}^{R}(\overline{P}_k^{(n)}(r)-\mu)^2}{R-1}} \tag{3}$$

where $\mu=\frac{1}{R}\sum_{r=1}^{R}\overline{P}_k^{(n)}(r)$ is the mean power over the realizations.

We distinguish two situations. First, the power variations across the array are removed using (4) (meaning that the

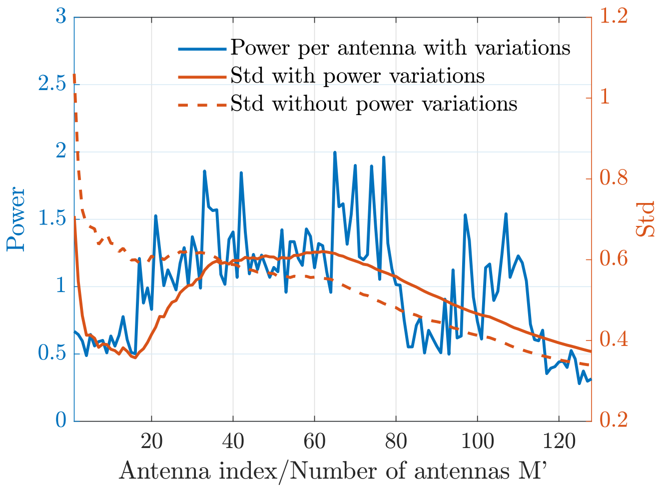

Fig. 8. Power of each antenna averaged over realizations. Standard deviation over realization of the average power in the subset of antennas, with and without removing the power variations across the array. NLoS Scenario, with User 1 antenna b in the first position.

power at each antenna averaged over all the measurements is the same). Second, the power variations across the array are maintained using the normalization described in (1).

In order to remove the power variations across the array the channel coefficient is normalized as follows:

$$\overline{h}_{mk}(r) = \frac{h_{mk}(r)}{\sqrt{\sum_{r=1}^{R}|h_{mk}(r)|^2}}\sqrt{R} \quad (4)$$

where $|\cdot|$ is the absolute value. This normalization creates a virtual power gain control that removes the user power imbalance and the differences among BS elements.

Fig. 8 shows the results of the standard deviation for both normalizations in the NLoS scenario and user 1 antenna b in the first position. The antennas are selected in a consecutive order starting from the right side of the array in Fig. 5. In addition the power of each antenna averaged over the channel realizations is presented. We observe that the channel hardening is affected by two factors. Adding more antennas with similar or less power reduces the standard deviation and adding more antennas with higher power increases the standard deviation. When a sufficient number of high power antennas is added then the law of large numbers becomes effective again. The first is a consequence of the law of large numbers and it contributes to the channel hardening of the massive MIMO channel. However, due to the large aperture of the massive MIMO arrays large power variations are observed across the array. These power variations can be detrimental for the channel hardening.

In Fig. 8 we see a decrease of the standard deviation for the first 16 antennas because their power is similar. The large power of the antennas 16 to 40 increases the standard deviation, which decreases after antenna 60 because the power of the antennas is reduced again. These effects are reduced in the standard deviation after removing the power variations across the array using the normalization presented in (4).

In the following we keep the power variations across the array using equation (1). In order to have more representative results, the standard deviation is averaged over all the positions of the subset of M' consecutive antennas over the array. The results are also averaged out over all the users.

First we focus on 64-mMIMO. Fig. 9 shows the standard deviation of the mean power in the S-LoS $\perp$ scenario. The results for a theoretical Gaussian channel are used as a reference.

The results show a decrease of channel variations when increasing the number of BS antennas. The VLA has the most hardening effect, followed by the LA which in turn is better than the C2D array. When the aperture of the array increases some of the antennas become more separated, which is likely to create less correlated channels and more hardening. We observe an increase in the standard deviation when the number of BS antennas is very high. The reason is the effect of power variations across the array. Even if we averaged for different positions of the subset of antennas, for a certain number of antennas M', the antennas in the middle of the array might be included more times in the subset than the antennas at the edges. However, when the number of antennas in the subset is small or large, all the antennas are included approximately the same number of times in the subset. For example, considering subsets of 1 antenna, each antenna in the array is included once. Considering subsets of 2 consecutive antennas, the first and last antennas of the array are are included in one subset, and the rest of the antennas are included in two subsets.

In order to have a broader view of the result, in Fig. 10 we plot the same metric for the maximum number of elements in the BS array (i.e. 64 antennas), taking the statistics across the 16 user antennas, for each array and scenario measured, which gives 16 samples per box. The boxplot shows the first and third quartiles as the bottom and top of the box, and the line inside the box is the second quartile (i.e. the median). The crosses in red are the outliers. Calling Q1 and Q3 the first and third quartiles, the outliers are the values below Q1-k(Q3-Q1) and above Q3+k(Q3-Q1). Here k= 1.5. The outliers depend on the value k and do not necessarily represent erroneous data. Here we use the boxplot to show the statistics of the data and not to find erroneous data. The median of the 16 user antennas shows that for all the scenarios, except the S-NLoS, the VLA has the strongest channel hardening, followed by the LA which in turn is better than the C2D. Thus, the conclusions obtained in Fig. 9 can be generalized in a statistical sense for most of the scenarios.

Second we focus on 128-mMIMO. We also keep the power variations across the array, and we average over all possible subsets of antennas and the different user antennas. Fig. 11 shows the standard deviation of the mean power in both LoS and NLoS scenarios. The Gaussian channel is also plotted as a reference. The results show a hardening effect in the channel. The standard deviation is larger for the NLoS scenario than for the LoS one.

In order to quantify the hardening we look at the ratio of the mean standard deviation obtained with 1 antenna to the mean standard deviation obtained with 128 antennas. In the Gaussian channel the ratio is 21 dB, while in the LoS it is 6 dB and in the NLoS it is 10 dB. Despite the differences between the Gaussian channel and the measured channels, the

This article has been accepted for publication in a future issue of this journal, but has not been fully edited. Content may change prior to final publication. Citation information: DOI 10.1109/TAP.2018.2871881, IEEE Transactions on Antennas and Propagation

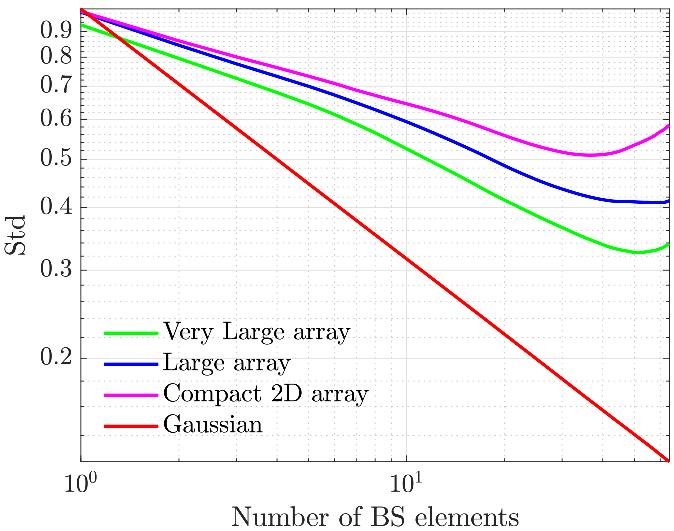

Fig. 9. Standard deviation of the mean power, averaged over subarray position and users, S-LoS ⊥

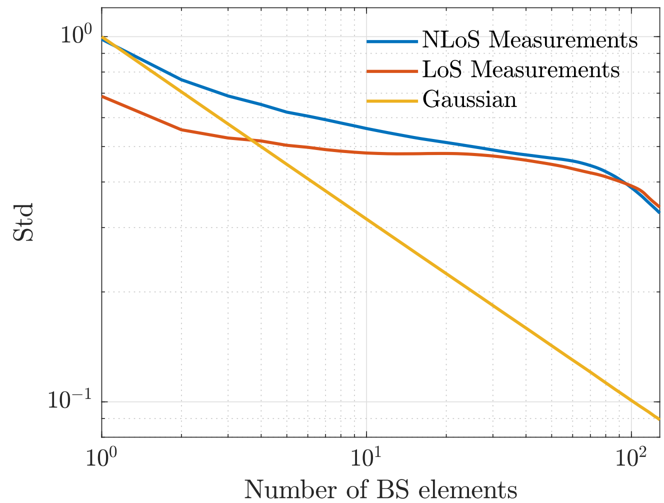

Fig. 11. Standard deviation of the mean power, averaged over subarray position and users, NLoS 0.57m and LoS 0.6m between users

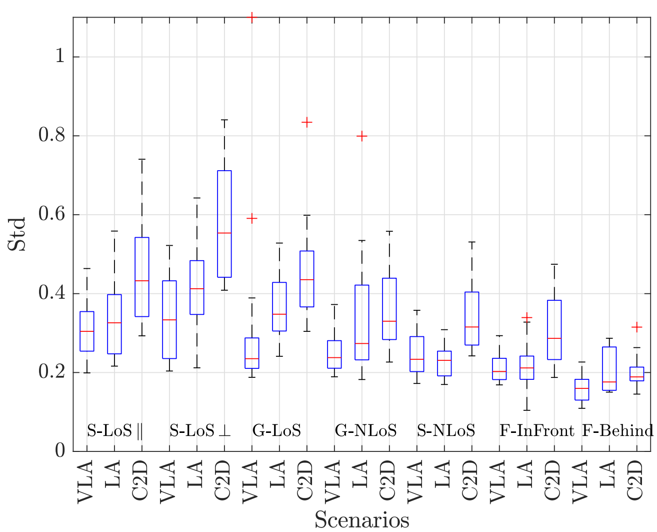

Fig. 10. Boxplot of the standard deviation of the mean power with 64 BS antennas, all the scenarios

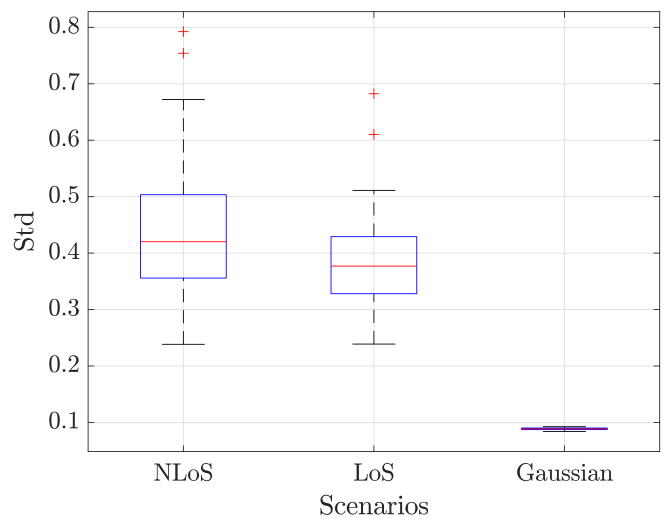

Fig. 12. Boxplot of the standard deviation of the mean power with 128 BS antennas

measured hardening is still significant.

In order to generalize the results, we look at the statistics over users and their positions. In Fig. 12 we show the same metric for 128 BS antennas taking the statistics over the 4 user antennas and all the measured positions of the users, which gives 84 samples for the NLoS scenario and the Gaussian channel boxes, and 40 samples for the LoS scenario box. We observe that the measured channels show a larger dispersion compared with the Gaussian channel as it is expected due to variation in the surroundings, hand grip, etc. We also observe the stronger hardening in the LoS scenario compared with the NLoS scenario. The NLoS scenario in some cases achieves as much hardening as the LoS but the median and the inter-quartile range is smaller for the LoS scenario.

As a conclusion, we observe the channel hardening effect when the number of BS antennas increases, but not as strong as for the Gaussian channel. We distinguish two effects that impact the channel hardening. First, if all the antennas of the array have similar power, adding more antennas increases the hardening. Second, if some antennas have higher power than the other antennas, the hardening is reduced. We also showed the improvement brought by increasing the aperture of the array, and the small impact of the LoS or NLoS scenarios.

V. Multi-user orthogonality and Sum-Rate

A. NLoS

The orthogonality between the channel vector of user k_1 and user k_2 is represented by its normalized scalar product,

$$SP(r) = \frac{\left|(\overline{\mathbf{h}}_{k_1}(r))^H \overline{\mathbf{h}}_{k_2}(r)\right|}{\left\|\overline{\mathbf{h}}_{k_1}(r)\right\| \left\|\overline{\mathbf{h}}_{k_2}(r)\right\|} \tag{5}$$

where $|\cdot|$ is the absolute value, and the superscript H denotes the conjugate transpose.

Fig. 13 shows the mean scalar product over the R realizations of the channel. First we put our attention into

This article has been accepted for publication in a future issue of this journal, but has not been fully edited. Content may change prior to final publication. Citation information: DOI 10.1109/TAP.2018.2871881, IEEE Transactions on Antennas and Propagation

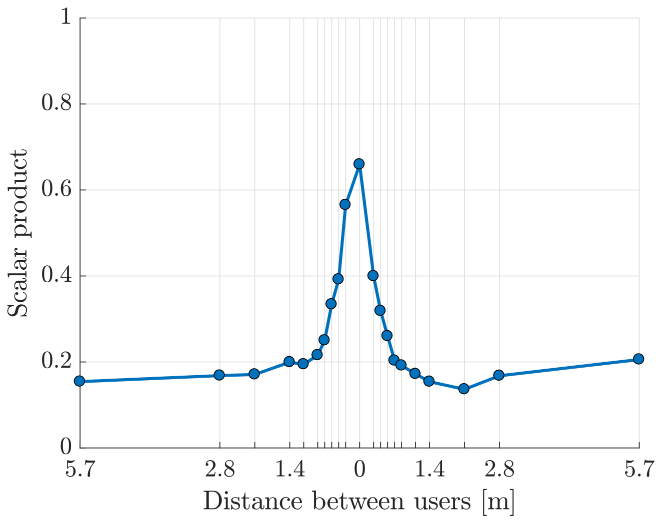

Fig. 13. Multi-user orthogonality, User 1 antenna a, User 2 antenna b, NLoS, 128-mMIMO

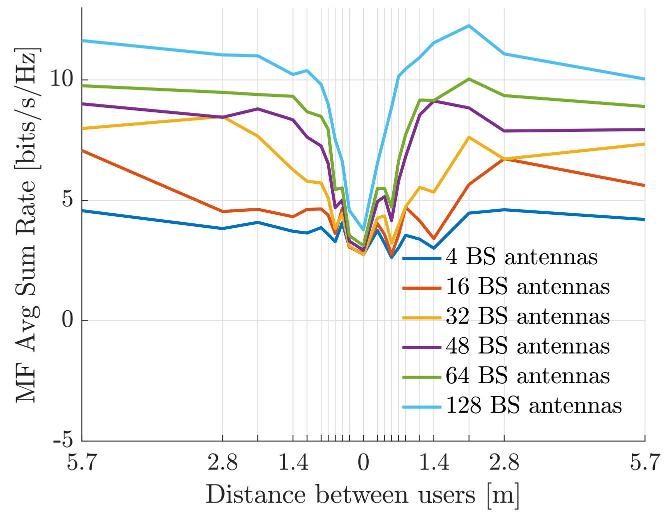

Fig. 14. Average sum-rate, User 1 antenna a, User 2 antenna b, NLoS, consecutive elements

the dependence of the channel vector orthogonality with the distance between users. When two users are placed in the same position their signals experience the same propagation phenomena (e.g. reflexion, diffraction, etc.). Therefore, the channels become highly correlated with a level up to 0.65. The channels are not exactly the same due to the handgrip of the users and small variations in the position since they cannot be at the same physical position. Increasing the distance between users decreases the inner product of their channel vectors. This result is complementary to the analysis in [17] section III.A. where the inner product between users is observed to decrease with the distance between users. About 0.2 correlation is observed for users separated more than approx. $1\,\mathrm{m}$ as also observed for well separated users and using 128 BS antennas in [4], [10].

The previous result on the inner product has a clear impact on the sum-rate of the system as linear precoders rely on the low correlation level of the users to simultaneously transmit independent data streams to them. Here we analyze the sum-rate of the system using the matched filter precoder.

The channel matrix is composed by the two channel vectors of the users using only one antenna

$$\overline{\mathbf{H}}(r) = [\overline{\mathbf{h}}_{k_1}^{(n_1)}(r) \quad \overline{\mathbf{h}}_{k_2}^{(n_2)}(r)] \tag{6}$$

The channel matrix $\overline{\mathbf{H}}(r)$ is normalized to achieve the desired average SNR.

$$\overline{\overline{\mathbf{H}}}(r) = \sqrt{\frac{R}{\sum_{r=1}^{R} \left\|\overline{\mathbf{H}}(r)^H \overline{\mathbf{H}}(r)\right\|_f^2}}\,\overline{\mathbf{H}}(r) \tag{7}$$

where $\|\cdot\|_f$ is the Frobenius norm.

We compute the SINR of each user considering an SNR of $15\,\mathrm{dB}$ as,

$$SINR_k = \frac{\alpha\left|\overline{\overline{\mathbf{H}}}_k \mathbf{W}_k\right|^2}{\alpha\left|\sum_{\substack{j=1\\ j\neq k}}^{K} \overline{\overline{\mathbf{H}}}_k \mathbf{W}_j\right|^2 + \sigma^2} \tag{8}$$

where $\mathbf{W}_i$ is the precoding vector for user i, $\overline{\overline{\mathbf{H}}}_i$ is the channel vector for user i, α is the normalization factor, and σ^2 is the power of the noise. The throughput for user k is computed as $R_k = \log(1 + \mathrm{SINR}_k)$. The sum rate is obtained summing the throughput R_k of all the users.

As expected, the sum-rate shown in Fig. 14 is strongly related to the inner product between user's channel vectors. When the users are in the same location the sum-rate drops nearly $50\,\%$ of that when they are well separated.

In the same figure we investigate the effect of increasing the number of BS elements from 4 to 128 while increasing the aperture. The elements are chosen in a consecutive order from the right side in Fig. 5. In the worst scenario presented (i.e. 4 BS elements) there is hardly an improvement as the inter-user distance increases. When the users are well separated, the improvement brought by an increase number of antennas is visible. This holds also true for a relatively close users, up to around $1\,\mathrm{m}$ separation. When the users become very closely spaced ($20\,\mathrm{cm}$ to $80\,\mathrm{cm}$), the impact of increase the number of antennas becomes much less significant.

The position of the elements (specially the aperture of the array, defined as the maximum distance between any two elements) plays a key role in defining the users' orthogonality. In the previous example the aperture of the array was increased at the same time as the number of elements. Next, we keep the aperture constant when increasing the number of elements. The results are presented in Fig. 15. In this figure two regions can be defined, namely an element limited region, and an aperture limited region. For arrays with more than 16 elements, the matched filter sum-rate is mainly defined by the aperture of the array, since the curves show a similar performance regardless the number of elements. The other region can be observed for the number of elements below 16. The matched filter sum-rate becomes limited by the number of elements, regardless the aperture of the array.

This article has been accepted for publication in a future issue of this journal, but has not been fully edited. Content may change prior to final publication. Citation information: DOI 10.1109/TAP.2018.2871881, IEEE Transactions on Antennas and Propagation

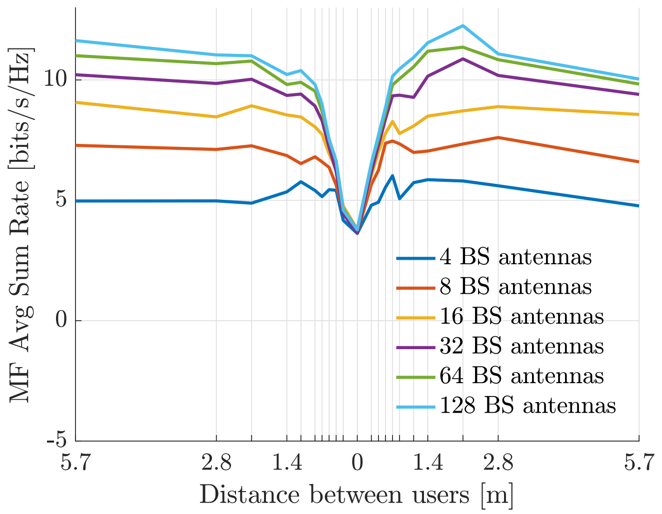

Fig. 15. Average sum-rate, User 1 antenna a, User 2 antenna b, NLoS, equidistant elements and fix aperture

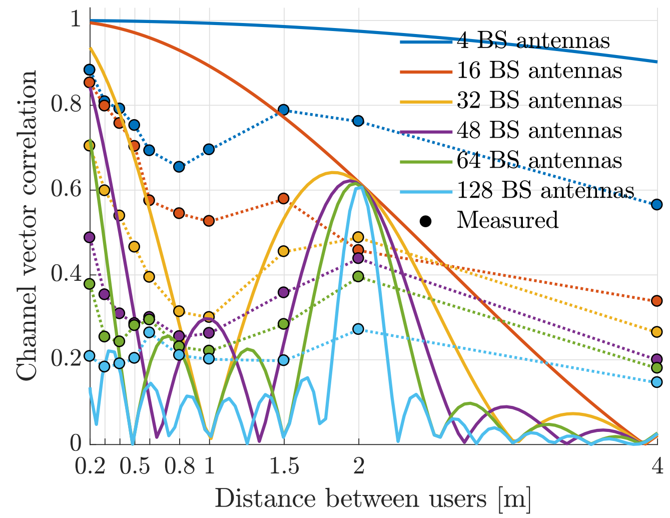

Fig. 16. Channel vector correlation, measured and simulated, User 1 antenna a, User 2 antenna b, LoS, consecutive elements

B. LoS

The matched filter sum-rate is also studied in the LoS scenario. In this scenario, the results are very related with the radiation pattern of the BS array, since the channel is dominated by the LoS component. For this reason, the sum-rate highly depends on the relative position of the users, with respect to the main beam and grating lobes. By observing Fig. 16, where we show the channel vector scalar product (as described in Eq. (5)) of a simulated scenario and the measured one, we see that the position of the BS elements strongly impacts the result. In the simulation, for 16 elements or less, there are no grating lobes, because the separation between consecutive elements is half the wave length. When the number of elements includes two sets of 16 elements, a correlation peak appears at $2\,\mathrm{m}$ separation between users due to the grating lobe. For an array with three sets, another peak of correlation appears, and so on. The measurements follow a similar pattern, with high correlation at $2\,\mathrm{m}$, lower correlation at $4\,\mathrm{m}$, etc. $4\,\mathrm{m}$ separated users are well-separated for large arrays that have narrow beams, so we observe similar correlations to [4], [10] of about 0.2. Smaller arrays have larger correlation than [4], [10] because our $4\,\mathrm{m}$ separation is smaller than the beamwidth, but their tenths of meters separation is larger.

Fig. 17 shows the matched filter sum-rate for the LoS scenario. First of all notice that for a user separation of $2\,\mathrm{m}$ the arrays with several sets (i.e. more than 16 elements) have a "valley" in the sum-rate due to the grating lobe, while the arrays with only one set (i.e. less or equal than 16 elements) do not see this effect. Especially in the curve of $32-$elements array, the symmetry with the previous figure (i.e. Fig. 16) is very clear. At separation $1\,\mathrm{m}$, the null in correlation translates to a high sum-rate. After these few examples it seems that in LoS the sum-rate is related with the radiation pattern of the BS array.

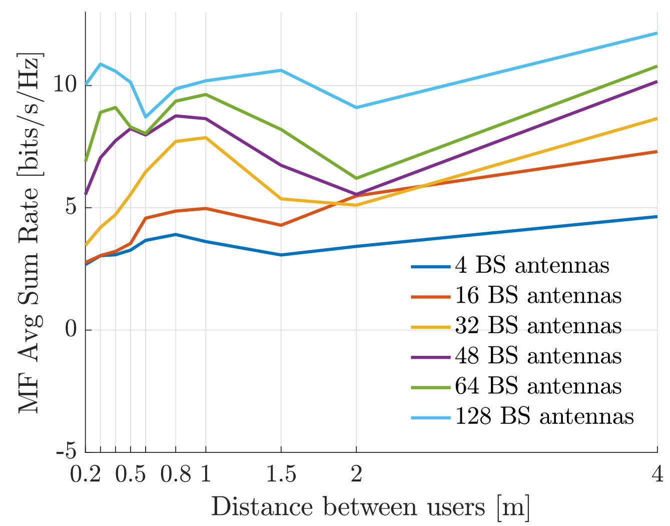

Fig. 17. Average sum-rate, User 1 antenna a, User 2 antenna b, LoS Parallel, consecutive elements

VI. Rank of the spatial covariance matrix

To investigate the rank of the spatial covariance matrix we compute the covariance matrix from the BS side

$$\mathbf{C}_k^{(n)} = \frac{1}{R}\sum_{r=1}^{R} \mathbf{h}_k^{(n)}(r)(\mathbf{h}_k^{(n)}(r))^H \tag{9}$$

Using an eigenvalue decomposition of the covariance matrix we obtain a set of eigenvalues $\Lambda = [\lambda_1 ... \lambda_{M'}]$, where M' is the number of selected BS elements. Fig. 18 shows the eigenvalue profile for user 1, antenna a, in all the 64-mMIMO measured scenarios with users.

For the LoS scenarios the total energy is generally concentrated on fewer eigenvalues, compared to the NLOS scenarios. For example a level of $-15\,\mathrm{dB}$ is reached at about 10 eigenvalues or less for the LoS scenarios, whereas about 20 eigenvalues are needed to reach that level in the NLoS scenarios. However, all the profiles are decaying smoothly, so that determining the

This article has been accepted for publication in a future issue of this journal, but has not been fully edited. Content may change prior to final publication. Citation information: DOI 10.1109/TAP.2018.2871881, IEEE Transactions on Antennas and Propagation

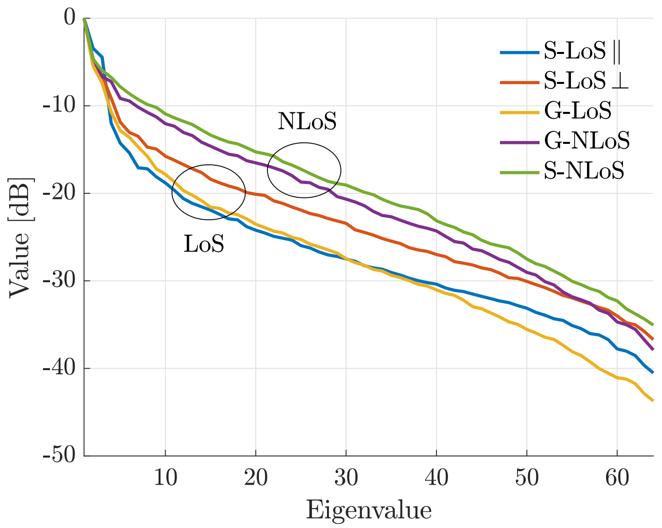

Fig. 18. Normalized eigenvalues profile, User 1 antenna a, C2D, all scenarios with user

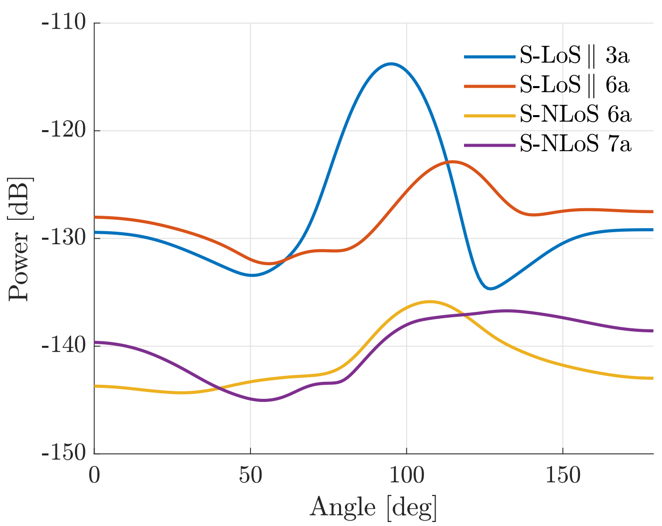

Fig. 19. Beamforming angle of arrival averaged over channel realizations, Large Array, set 3

rank of the spatial covariance matrix effectively depends on the choice of threshold.

The smoothness of the curves can be attributed to limitations of practical measurements such as the limited number of measurements, a degree of non-stationarity of the channel, and inevitable imperfections like noise and spurious signals.

Insight into the channel rank properties can also be gained by analysing angle of arraivals. Fig. 19 shows average beamforming spectra (Hamming weighted) obtained with the LA, Set 3 in both LoS and NLoS with different users. While it is possible to identify a main angle of arrival for the case of a nearby LOS user, it is also clear that the distribution over angle is much more even in the NLOS scenarios, as expected from the eigenvalue distributions in Fig. 18. Even if the users have a dominant path, we observe energy scattered in other angles, as also reported in [3], [5].

VII. Conclusion

This paper investigates three major characteristics of massive MIMO channels that are widely accepted and used in most of the theoretical studies, but they have, to the best of our knowledge, never been verified in measured propagation channels. These characteristics are the channel hardening in terms of mean power across the array, user orthogonality for specific distances between users and the rank of the spatial covariance matrix.

The presented results confirm the channel hardening effect of the massive MIMO channels. The study shows how the standard deviation of the mean power across the BS array decreases when the number of elements in the array increases, but only if they have similar power level. We also show the stronger hardening brought by increasing the aperture of the array.

This study also shows the sum-rate of the matched filter precoder of two users separated certain distances. The results show that in NLoS scenarios, the sum-rate decreases when the users are close to each other. In LoS scenarios the sum-rate depends on the exact position of the users respect to the beam created by the array. It makes clear the importance of taking into account the distance between users to model the system.

Finally in the study on the rank of the spatial covariance matrix, the profile of eigenvalues of the covariance matrix does not show a clear group of effective eigenvalues. Looking at the angle-of-arrival of the signal it is clear the energy is scattered in multiple directions, except in LoS with users very close to the BS array.

Acknowledgment

The research presented in this paper was supported by the Danish Council for Independent Research (Det Frie Forskningsråd) DFF133500273 and the Danish National Advanced Technology Foundation via the VIRTUOSO project.

References

[1] A. Osseiran, J. F. Monserrat, and P. Marsch, *5G Mobile and Wireless Communications Technology*, 1st ed. Cambridge University Press, Oct. 2016.

[2] T. L. Marzetta, "Noncooperative cellular wireless with unlimited numbers of base station antennas," *IEEE Transactions on Wireless Communications*, vol. 9, no. 11, pp. 3590–3600, 2010.

[3] S. Payami and F. Tufvesson, "Channel measurements and analysis for very large array systems at 2.6 GHz," *2012 6th European Conference on Antennas and Propagation*, pp. 433–437, 2012.

[4] J. Hoydis, C. Hoek, T. Wild, and S. ten Brink, "Channel measurements for large antenna arrays," *2012 International Symposium on Wireless Communication Systems (ISWCS)*, pp. 811–815, 2012.

[5] L. Wenjuan, L. Liu, T. Cheng, L. Yanping, X. Jingcheng, and L. Pengyu, "Channel measurements and Angle Estimation for Massive MIMO Systems in a Stadium," *Advanced Communication Technology (ICACT), 2015 17th International Conference on*, pp. 3–6, 2015.

[6] D. Fei, R. He, B. Ai, B. Zhang, K. Guan, and Z. Zhong, "Massive MIMO Channel Measurements and Analysis at 3.33 GHz," *10th International Conference on Communications and Networking in China*, pp. 194–198, 2015.

[7] H. Yu, Q. Zheng, Z. Zheng, L. Tian, and Y. Wut, "The Rationality Analysis of Massive MIMO Virtual Measurement at 3.5 GHz," *Communications in China (ICCC Workshops), 2016 IEEE/CIC International Conference on*, 2016.

This article has been accepted for publication in a future issue of this journal, but has not been fully edited. Content may change prior to final publication. Citation information: DOI 10.1109/TAP.2018.2871881, IEEE Transactions on Antennas and Propagation

[8] J. Li, B. Ai, R. He, K. Guan, Q. Wang, D. Fei, Z. Zhong, Z. Zhao, D. Miao, and H. Guan, "Measurement-based characterizations of indoor massive MIMO channels at 2 GHz, 4 GHz, and 6 GHz frequency bands," *IEEE Vehicular Technology Conference*, vol. 2016-July, pp. 4–8, 2016.

[9] J. Chen, X. Yin, and S. Wang, "Measurement-based Massive MIMO Channel Modeling in 13 - 17 GHz for Indoor Hall Scenarios," *Communications (ICC), 2016 IEEE International Conference on*, vol. 1, no. 61471268, pp. 1–5, 2016.

[10] G. Xiang, O. Edfors, F. Rusek, and F. Tufvesson, "Linear Pre-Coding Performance in Measured Very-Large MIMO Channels," *Vehicular Technology Conference (VTC Fall), 2011 IEEE*, pp. 1–5, 2011.

[11] M. Gauger, J. Hoydis, C. Hoek, H. Schlesinger, A. Pascht, and S. ten Brink, "Channel Measurements with Different Antenna Array Geometries for Massive MIMO Systems," *SCC 2015; 10th International ITG Conference on Systems, Communications and Coding; Proceedings of*, pp. 1–6, 2015.

[12] J. Flordelis, X. Gao, G. Dahman, F. Rusek, O. Edfors, and F. Tufvesson, "Spatial Separation of Closely-Spaced Users in Measured Massive Multi-User MIMO Channels," *Communications (ICC), 2015 IEEE International Conference on*, pp. 3044–3049, 2015.

[13] X. Gao, F. Tufvesson, O. Edfors, and F. Rusek, "Measured propagation characteristics for very-large MIMO at 2.6 GHz," *2012 Conference Record of the Forty Sixth Asilomar Conference on Signals, Systems and Computers (ASILOMAR)*, pp. 295–299, 2012.

[14] X. Gao, O. Edfors, F. Rusek, and F. Tufvesson, "Massive MIMO Performance Evaluation Based on Measured Propagation Data," *IEEE Transactions on Wireless Communications*, vol. 14, no. 7, pp. 3899–3911, 2015.

[15] M. Teeti, J. Sun, D. Gesbert, and Y. Liu, "The Impact of Physical Channel on Performance of Subspace-Based Channel Estimation in Massive MIMO Systems," *IEEE Transactions on Wireless Communications*, vol. 14, no. 9, pp. 4743–4756, 2015.

[16] A. Adhikary, J. Nam, J.-Y. Ahn, and G. Caire, "Joint Spatial Division and Multiplexing," *IEEE Transactions on information theory*, vol. 59, no. 10, pp. 6441–6463, 2013.

[17] À. Oliveras Martínez, E. D. Carvalho, and J. Ø. Nielsen, "Towards Very Large Aperture Massive MIMO : a measurement based study," *Globecom Workshops (GC Wkshps), 2014*, pp. 281–286, 2014.

[18] À. Oliveras Martínez, E. D. Carvalho, J. Ø. Nielsen, and L. Jing, "Frequency Dependence of Measured Massive MIMO Channel Properties," *Vehicular Technology Conference (VTC Spring), 2016 IEEE 83rd*, 2016.

[19] À. Oliveras Martínez, E. De Carvalho, and J. Ødum Nielsen, "Massive MIMO Properties based on Measured Channels : Channel Hardening, User Decorrelation and Channel Sparsity," *Conference Record of the Fiftieth Asilomar Conference on Signals, Systems and Computers*, 2016.

[20] B. M. Hochwald, T. L. Marzetta, and V. Tarokh, "Multiple-antenna channel hardening and its implications for rate feedback and scheduling," *IEEE Transactions on Information Theory*, vol. 50, no. 9, pp. 1893–1909, 2004.